Pulse Nuclear Magnetic Resonance Study of ^{1}H and ^{19}F

Bhaskar Mookerji and Charles Herder*
MIT Department of Physics, 8.13
(Dated: March 2, 2008)

We examine nuclear magnetic resonance (NMR) phenomena in an ensemble of spin-1/2 particles by altering the magnetization of glycerin, hexaflourobenzene, and ferric(II) chloride in a static magnetic field with carefully timed RF pulses. At resonance, we determine the gyromagnetic ratios of the proton and flourine as $2\pi\times(23.9+4.9-1.5)\times10^3\mathrm{G}^{-1}\mathrm{Hz}$ and $2\pi\times(22.8+4.5-1.6)\times10^3\mathrm{G}^{-1}\mathrm{Hz}$, within experimental error of accepted values. Correlations of viscosity and paramagnetic ion doping to thermal and transverse relaxation times T_1 and T_2 are confirmed, but differ quantitively from earlier results. The inhomogeneity of the static field is given by $\Delta H_0 = 0.28 \pm 0.15\mathrm{G}$.

The theory of nuclear magnetic resonance (NMR) was developed independently by Bloch and Purcell, and later modified by Hahn's description of spin echoes and the Carr-Purcell method. NMR uses the intrinsic spin magnetic moment of atomic nuclei to identify various atomic and solution properties for medical imaging and analytical chemistry applications [1]. Following this work, we first describe the theory of pulsed NMR. We then measure the intrinsic magnetic moments of the ^{1}H and ^{19}F nuclei and characterize the effects of solution properties such as viscosity and paramagnetic ion doping on the resonance properties of these nuclei.

1. RESONANCE AND PHASE DECOHERENCE

NMR describes the resonant behavior of a spin-1/2 particle in a time-varying magnetic field. Our ultimate goal is to measure the resonant frequency ω_0 associated its magnetic moment μ and the time-scale of its decoherence. The particle is described as a *qubit* state in terms of the S_z spin eigenstates $\left|\frac{1}{2}\frac{1}{2}\right\rangle = |\uparrow\rangle$ and $\left|\frac{1}{2}\frac{-1}{2}\right\rangle = |\downarrow\rangle$:

$$|\psi(t)\rangle = a_+(t)\,|\uparrow\rangle + a_-(t)\,|\downarrow\rangle\,. \tag{1}$$

The interaction of an external magnetic field $\mathbf{B}$ with the two-state spin given is described by the Hamiltonian

$$H = -\mu\cdot\mathbf{B}, \tag{2}$$

where $\mu = \gamma\mathbf{S}$ is the magnetic moment associated with the particle's gyromagnetic ratio γ and total spin $\mathbf{S}$. Initially, an ensemble average of these particles are in thermal equilibrium at room temperature, and a finite energy gap between the spin eigenstates of a given particle results in a Maxwell-Boltzmann distribution for the relative populations of particles in the two spin states. A greater proportion are in the $|\uparrow\rangle$ state, and thus the application of a large, static magnetic field $B_0\hat{e}_z$ causes Larmor precession about $\hat{e}_z$ with frequency $\omega_0 = \gamma B_0$ as described by Ehrenfest's Theorem:

$$\frac{\partial\langle\mu\rangle}{\partial t} = -\frac{i}{\hbar}\langle[\mu, H]\rangle = \gamma\langle\mu(t)\rangle\times\mathbf{B}(t)\,. \tag{3}$$

The qubit state of the system is manipulated at resonance by applying a weak, time-oscillating field $B_1\,(\hat{e}_x\cos\omega t - \hat{e}_y\sin\omega t)$ orthogonal to $\mathbf{B}_0$. Using total static and varying fields, Equation 2 can be written as

$$H = \frac{\hbar}{2}\begin{pmatrix}\omega_0 & \omega_1 e^{-i\omega t}\\ \omega_1 e^{i\omega t} & -\omega_0\end{pmatrix} \tag{4}$$

in the $\{|\uparrow\rangle, |\downarrow\rangle\}$ basis, where $\omega_1 = \gamma B_1$. Transforming into a frame rotating about the $\hat{e}_z$ with frequency ω_0 using $|\phi(t)\rangle = e^{i\omega t S_z/\hbar}\,|\psi(t)\rangle$, Equation 4 becomes a rotating-frame Hamiltonian

$$\tilde{H} = \frac{\hbar}{2}\begin{pmatrix}-\Delta\omega & \omega_1\\ \omega_1 & \Delta\omega\end{pmatrix} \tag{5}$$

which describes a single qubit's magnetic moment nutating about $\hat{e}_z$. When the applied frequency ω of the time-varying field differs substantially from the Larmor frequency ω_0, the qubit's time-evolution is identical to the $\mathbf{B}_0$ Hamiltonian. However, at resonance ($\Delta\omega \approx 0$), the $\mathbf{B}_0$ is negligible in comparison to the $\mathbf{B}(t)$ which causes large rotations about the $\hat{e}_x$ axis. In this way, the time-varying field can be pulsed for short periods to alter nuclear spin states. Applying this field for time t, the probability of measuring $|\downarrow\rangle$ from an initial state $|\uparrow\rangle$ yields the Rabi equation:

$$|\langle\downarrow|\phi(t)\rangle|^2 = \frac{\omega_1^2}{\omega_1^2 + (\Delta\omega)^2}\sin^2\left[\frac{1}{2}\sqrt{(\Delta\omega)^2+\omega_1^2}\,t\right]. \tag{6}$$

Pulsing an initial state $|\uparrow\rangle$ into $|\downarrow\rangle$ with unity probability requires that $t = \pi/\gamma B_1$ and is known as a π-pulse; a pulse for $t = \pi/2\gamma B_1$ is known as a $\pi/2$-pulse.

In reality, the final state of our system returns to its thermal equilibrium state and decoheres due to effects within the sample through free induction decay (FID). From it's final state our system approaches thermodynamic equilbrium toward a magnetization $\mathbf{M}_0$ from field $\mathbf{B}_0$. An energy density $-\mathbf{M}\cdot\mathbf{B}$ is exchanged with system's other degrees of freedom (*lattice*) and a longitudinal relaxation occurs in time T_1. Bloembergen related this time to the viscosity η and concentration N_{ion} of a solution with paramagnetic ion μ_{eff},

$$\frac{1}{T_1} = \frac{12\pi\gamma^2\eta N_{\mathrm{ion}}\mu_{\mathrm{eff}}^2}{5k_BT} \tag{7}$$

*Electronic address: mookerji@mit.edu, cherder@mit.edu

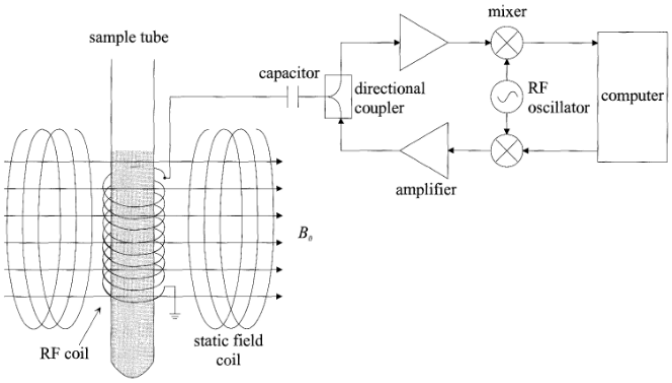

FIG. 1: Pulse NMR probe and signal chain. A 50Ω impedance-matched LC circuit made from wound #18 copper wire (10 times, 2cm×10mm) and two tunable shunt capacitors applies an RF pulse to a $1cm^3$ sample in a glass cuvette. Larmor precession is induced in the xy-plane and the resultant alternating magnetic flux returns an RF voltage from the sample into the signal chain. A static field B_0 is produced by a 1775.7 Gauss hard magnet [1].

A transverse relaxation results from the destructive interference of phase coherence from disparate spin precessions. This spread in spin precessions comes from two effects. In addition to the static field B_0, each spin experiences a smaller dipole field from from the interaction of magnetic moments. The transverse relaxation time to field alignment for only this effect is T_2. An additional static field inhomogeneity ΔH_0 shortens this relaxation time and is given by T_2^*:

$$\frac{1}{T_2^*} = \frac{1}{T_2} + \gamma \Delta H_0. \tag{8}$$

2. EXPERIMENTAL SETUP AND PROCEDURE

We performed pulsed NMR experiments on a pre-prepared samples of glycerin (100%, 95%, 75%, 60%, 50%, and 25% by mass at 23.6 ± 0.5°C), hexafluorobenzene (C_6F_6), tap and distilled water, and distilled water doped with the paramagnetic ion $FeCl_3 \cdot 6H_2O$ (45gm/mL). A diagram depicting this sample preparation is found in Figure 1. A digital pulse programmer controls the pulse width, delay time (τ), and repeat time of desired RF pulse sequences of the transverse field B_1 to millisecond precision by sending TTL pulses to an RF switch. The transverse field itself is driven by an 80MHz Agilent 33250A function generator producing a +10dBm sine wave in the resonance region of a sample. Half of this signal is fed to a 2W RF amplifier to +33dBm and sent to the sample probe switch; the remainder is reference for the phase detector. The resulting RF voltage from the sample probe is passed to a Tron-Tech W110F pre-amplifier and 7MHz bandpass filter, and ultimately compared to the reference signal with a Mini-Circuits ZRPD-1. Beats from the mixed signal are displayed 60MHz Agilent 54621A oscilloscope and digitized by a PC over GPIB. Impedance matching is achieved by with an signal output and RF power input. Crossed diodes were added between the sample probe and ground, and between the signal pre-amplifier input and ground in order to isolate the pre-amplifier and ground strong RF pulses at the output.

Adjustable parameters in this experiment were largely limited to pulse and FID timing parameters. To minimize magnetic field inhomogeneity ΔH for the longitudinal field, the position of the sample probe was laterally altered until the qualitative length of the FID was maximized. The π-pulse width (approx. 30ms) was determined by picking the first time that minimized the FID, from which the $\pi/2$-pulse was chosen to be exactly half. Repeat timing was sufficiently long for the sample to reach equilibrium state between pulses.

Magnetic moment and spin relaxation times were measured by the application of spin-echo and Carr-Purcell pulse sequences to our samples. The magnetic moments of ^1H and ^{19}F were determined by measuring the Larmor frequency of pure glycerin and hexaflourobenze in a known magnetic field. We excited our sample with a $\pi/2$-pulse off resonance and measured the beat frequency of its FID. The applied field B_0 was measured using a RFL 912 Hall gaussmeter and calibrated by a zero-field source. To ensure that the measured field was not affected by the angle of the Hall probe, we measured the field by slowly rotating the probe until a maximum was found.

The thermal relaxation time T_1 was measured using the three-pulse sequence $\pi - \tau - \pi/2 - \pi$ which inverts the excess spin population following a π-pulse, allowing them to reach equilibrium. As τ is increased, the amplitude of the FID following the remaining pulse increases and causes zero at time $T_1 \ln 2$. Plotting echo height versus τ and fitting the form $A\left(1 - e^{-\tau/T_1}\right)$ estimates the decay constant.

The two transverse relaxation times T_2^* and T_2 are determined from the π-pulse FID and spin-echo sequences respectively. The transverse relaxation time T_2^* was measured from the FID decay constant of a $\pi/2$-pulse and checked against the line width $2/T_2^*$ of its Fourier transformation. The effect of the inhomogeneity ΔH is controlled by a $\pi/2 - \tau - \pi$ pulse sequence that refocus magnetization with a second pulse in time interval 2τ. The resulting echo heights are described by

$$E(2\tau) = E(0) \exp\left[-\frac{2\tau}{T_2} - \frac{2}{3}\gamma^2 G^2 D \tau^3\right], \tag{9}$$

where D and G are the diffusion constants and magnetic field gradient characterizing the magnetization response of a viscous sample. We used an $\pi/2 - (\tau - \pi - \tau)_n$ Carr-Purcell pulse train to minimize the effects of viscosity on echo height with height of the nth pulse given at $t = n\tau$. In order to minimize the effect of diffusion on echo heights, as many pulses were taken as possible with values of τ ranging between 1 and 10ms ($n \approx 50 \ldots 180$) so that an purely exponential decay determined T_2. Large

pulse counts are particularly important here, as the Carr-Purcell pulse train introduces a cumulative error due to the inhomogeneity of the transverse B_1 field and repeated $\pi-$pulses departing from ideality; subsequent measured T_2, will be underestimated [2]. With this in mind, we applied as many π-pulses as possible while still allowing adequate τ to reach equilibrium. We will further account for this error in Section 3.

3. RESULTS AND ERROR ANALYSIS

Uncertainties in our determination of voltage pulse sequences were mostly systematic and instrumental in nature. At the maximum sample rate, the instrumental uncertainty in our oscilloscope was on the order of 1mV. Digitized oscilloscope traces introduced an additional sampling error of 0.04mV and $13\mu s_{\mathrm{RMS}}$ in sampled voltage pairs, although this error was ultimately insignificant. A standard Hall gauss-meter probe was used to measure the field and results in a variation of approximately 30 gauss. Accounting for a possible overestimate of the true value due to our method of Hall measurement, the maximum error is closer to 60 Gauss, corresponding to maximum error of 0.03×10^6rad/sec and a minimum error of half this value. Natural line width as an error source in resonance determination is dominated by the error due to magnetic field inhomogeneity, which will ultimately be extrapolated from our data. Finally, spectral analysis of hexafluorobenzene a with weak voltage response adds another 1.5×10^3rad/sec error in our determination of ^{19}F resonance.

Errors in T_1, T_2, and T_2^* are 1σ errors determined from an LMA nonlinear fitting algorithm in Mathematica 6. Added in quadrature to the fitting error in T_2 is the systematic rms error inherent to the Carr-Purcell procedure. It has been shown that the rms error in a pulse train will fall off as $\sqrt{n}$, where n is the number of π pulses applied in T_2. Therefore, calculated errors for a *measured* T_2 were added in quadrature to 1σ errors in fit as $T_2/\sqrt{n}$, where n ranged between 50 and 180 pulses [2].

3.1. Resonance of ^{1}H and ^{19}F

Figure 3.1 depicts sample FID data used to determine resonance frequency of hydrogen in this experiment. The resonant frequency of the proton was determined by driving a pure glycerin sample off-resonance at ω_{app} by a π-pulse and measuring its FID. To minimize spectral leakage of higher frequency components beyond the desired frequency range, we multiplied the FID by a Bartlett-Hann window function and then took its Fourier transform to measure the beat frequency $\Delta\omega = \omega_{\mathrm{app}} - \omega_0$. The measured magnetic moment of ^{19}F and ^{1}H are determined as $(40.5 + 0.3 - 0.003) \times 10^6$rad/sec and $(42.5 + 0.3 - 0.002) \times 10^6$rad/sec, each within 1σ of the accepted values of 40.8rad/sec and 42.5781rad/sec. Gyromagnetic ratios were determined to be $2\pi \times (23.9 + 3.9 - 1.5) \times 10^3 \mathrm{G}^{-1}\mathrm{Hz}$ and $2\pi \times (22.8 + 3.5 - 1.6) \times 10^3 \mathrm{G}^{-1}\mathrm{Hz}$ from the static field B_0

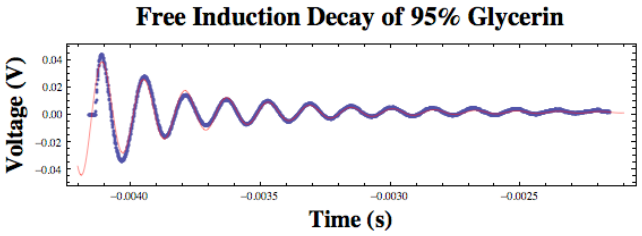

(a)FID of 95% Glycerin

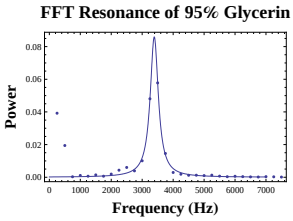

(b)Windowed FFT at beat frequency $\Delta\omega$.

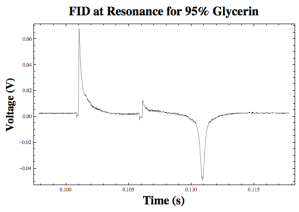

(c)Protons at resonance.

FIG. 2: Sample measurement of the Larmor frequency of ^{1}H from 95% glycerin. The driving frequency in (c) directly measures the resonant frequency ω_0. χ^2 tests of fits for sample FIDs and resonance curves ranged from 0.5 to 2.

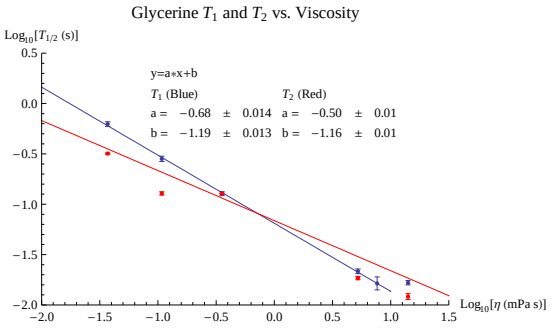

FIG. 3: Dependence of relaxation time on viscosity at $23.6 \pm 0.5°$C.

3.2. Relaxation Times

Plots of T_1 and T_2 dependence on viscosity and paramagnetic ion doping are found in Figures 3 and 4 and aggregate relaxation times can be found in Table I. Our values of T_1 depend on viscosity η and N_{ion} as -0.68 and -1.30, differing from the -1 dependence described by Bloembergen in Equation 7. These T_1 correlations are overestimated, as samples are operating in the saturation region of viscosity dependence where time scale of relaxation approaches that of thermal oscillations in the lattice.

A damped oscillator was fit to the FIDs of our samples to determine T_2^* and checked against the line width $2/T_2^*$

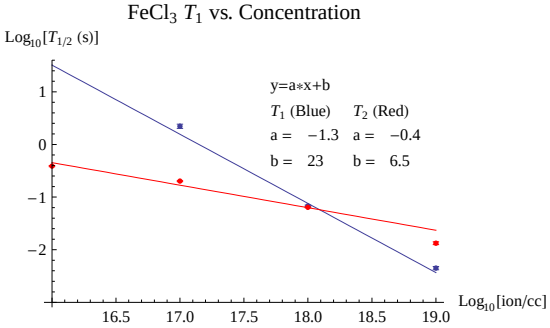

FIG. 4: Dependence of relaxation time on paragmagnetic doping concentration.

TABLE I: Longitudinal and transverse relaxation time at $23.6 \pm 0.5°$C. Ion concentrations are in ions/cc.

η (%)	T_1 (ms)	T_2 (ms)	T_2^* (ms)	ΔH_0 (Gauss)
100	16.6 ± 0.4	12.13 ± 1.72	0.44 ± 0.07	0.23 ± 0.09
95	21.6 ± 0.5	18.50 ± 1.93	0.51 ± 0.07	0.24 ± 0.08
75	128.0 ± 2.5	127.8 ± 6.23	0.99 ± 0.13	0.28 ± 0.04
60	283.0 ± 7.4	128.0 ± 8.89	0.51 ± 0.08	0.53 ± 0.06
40	620 ± 15	318.4 ± 9.52	0.74 ± 0.09	0.80 ± 0.11
25	–	410.6 ± 26.3	0.83 ± 0.10	0.14 ± 0.11
$[FeCl^{3+}]$				
10^{19}	4.50 ± 0.14	13.31 ± 1.82	–	–
10^{18}	67.0 ± 1.1	63.72 ± 5.15	–	–
10^{17}	2200 ± 90	201.5 ± 9.49	–	–
10^{16}	–	386.70 ± 9.56	–	–

of its Fourier transformation, which generally agreed. An exponential decay was fit to the decaying echo heights taken the scope trace of a Carr-Purcell sequence. Fits for these were quite good (χ^2 ranged between 0.5 and 2). Accounting for a possible outlier, the inhomogeneity of the field ΔH_0 is extrapolated by 0.28 ± 0.15G using Equation 8. The relative magnitude in this error is not surprising, as ΔH_0 is dependent on the positioning of the sample.

Spin-spin relaxations are affected by the correlation time of interaction between magnetic moments in a given sample. A less viscous sample will be more likely to diffuse due to a given magnetic field gradient, and so transverse relaxation times for viscous substances will be far shorter than less viscous ones. We expect, therefore, for transverse relaxation times to decrease for a given viscosity. A identical trend is predicted when considering a paramagnetic solute in a sample. Dipole fields from unpaired electrons in $FeCl_2$ causes magnetization to decay far more quickly, and so relaxation times should decrease with greater solute concentration. The trend in Figures 3 and 4 indicates this is true for both factors, but differs from the -1 as predicted by Bloombergen [3]. This is not particularly surprising, as the actual concentrations in both cases were assumed to be true, and subsequent evaporation of water, oxidation of $FeCl_2$ into rust, and presence of atmospheric oxygen may have contaminated our sample. Issues regarding the purity of these samples are discussed in Section 4 this paper.

The $T_1 \approx T_2$ values for tap and distilled water were measured to 1.90 ± 0.03s and 2.13 ± 0.04s, respectively. This differ from Bloembergen's measurement of 2.3s, which is not particularly surprising when accounting for the presence of free ions in tap water and the presence of dissolved, paramagnetic O_2 in both samples. Greater spin-lattice interaction in these samples shortened their longitudinal relaxation times. An attempt to remove oxygen by bubbling N_2 yielded unreasonable relaxation time, suggesting that bubbles were trapped within the sample.

4. DISCUSSION

It is not a surprise that details of sample preparation should be an area of focus for future groups doing the lab. Follow-up works to Bloombergen's thesis have differed substantially in their determinations of relaxation times in glycerin, and have even suggested that his samples may have had at least 2% contamination with water [4]. Glycerin samples could be heated (80°C) under inert vacuum and stored within a desiccator to prohibit contamination from atmospheric oxygen and water. Also, errors in the Carr-Purcell determination dominate the error in determination of transverse relaxation time, and further shallow its dependence on viscosity and paramagnetic ion doping. Discounting sample contamination, accurately measuring T_2 to with 1% of accepted values would require at least 10^4 pulses in a sequence, well beyond the capability of the pulse programmer. In these ways, it might be very well impossible to accurately measure such relaxation times without serious modification well beyond the scope of the current lab. Adding a programmer for controlling pulse phase may solve this issue with allowing the Carr-Purcell sequence to be modified to the Carr-Purcell-Meiboom-Gill sequence [2]. Also, introducing a colorimeter to measure solute concentration through absorption spectroscopy would similarly improve the ion doping experiment [5][6].

[1] M. Nielsen and I. Chuang, *Quantum Computation and Quantum Information* (Cambridge University Press, 200).
[2] H. Pursey, Proc. Phys. Soc **78**, 808 (1961).
[3] E. M. P. N. Bloembergen and R. Pound, Phys. Rev. **73**, 679 (1948).
[4] J. K. K. Luszczyski and J. Powles, Proc. Phys. Soc **75**, 243 (1960).
[5] *Brinkman 600 Portable Colorimeter for ˜$100* (????), URL http://www.labx.com/v2/newad.cfm?catID=132.
[6] *B. Mookerji thanks C. Herder for his equal contribution to the this experiment and its analysis, the Junior Lab staff, and Mark Tobenkin for remarks on signal processing.*